Characterisation of immune cell subsets of tumour infiltrating lymphocytes in brain metastases

Priyakshi Kalita-de Croft[1]*, Haarika Chittoory[1], Tam Nguyen[4], Jodi M Saunus[1], Woo Gyeong Kim[1#], Amy McCart Reed[1], Malcolm Lim[1], Xavier M De Luca[1], Kaltin Ferguson[1], Colleen Niland[1], Roberta Mazzieri[3,5], Riccardo Dolcetti[3,5], Peter T Simpson[1], Sunil R Lakhani[1,2*]

[1]The University of Queensland Faculty of Medicine, UQ Centre for Clinical Research, Herston, Queensland, Australia

[2]Pathology Queensland, The Royal Brisbane and Women's Hospital Herston, Queensland, Australia

[3]The University of Queensland Diamantina Institute, Brisbane, Queensland, Australia

[4]QIMR Berghofer research institute, Herston, Queensland, Australia

[5]Sir Peter MacCallum Cancer Centre, University of Melbourne, Parkville, VIC 3010, Australia

#Permanent address: University of Inje College of Medicine, Dept of Pathology, Haeundae Paik Hospital, Busan, South Korea

*Correspondence: p.kalita@uq.edu.au; s.lakhani@uq.edu.au; Tel.: (+61 73346 6048)

Abstract: The heterogeneity of tumor infiltrating lymphocytes is not well characterized in brain metastasis. To address this, we performed a targeted analysis of immune cell subsets in brain metastasis tissues to test which immunosuppressive routes are involved in brain metastasis. We performed multiplex immunofluorescence (mIF), using commercially available validated antibodies on twenty formalin-fixed paraffin embedded whole sections. We quantitated the subsets of immune cells utilizing a targeted panel of proteins including PanCK, CD8, CD4, VISTA and Iba1, and analyzed an average of 15000 cells per sample. We classified tumours as either high (>30%) or low (<30%) tumour infiltrating lymphocytes (TILs) and found that increased TILs density correlated with survival. We next sought out to phenotype these TILs using mIF. The tumours with low TILs (n=9) had significantly higher expression of the immune-checkpoint molecule VISTA in tumor cells (p<0.01) as well as in their microenvironment (p<0.001). Contrastingly, the brain metastatic tumours with high TILs (n=8) displayed higher levels of activated microglia, as measured by Iba1 expression. Low TILs-tumours displayed CD8+ T-cells that co-express VISTA (p<0.01) significantly more compared to high TILs group, where CD8+ T-cells significantly co-express Iba1 (p<0.05). Interestingly, no definite phenotypes of CD4+ subsets were observed. These results were supported by RNA analysis of a publicly available, independent cohort. In conclusion, our work contributes to a growing understanding of the immune surveillance escape routes active in brain metastasis.

39   **Graphical Abstract**
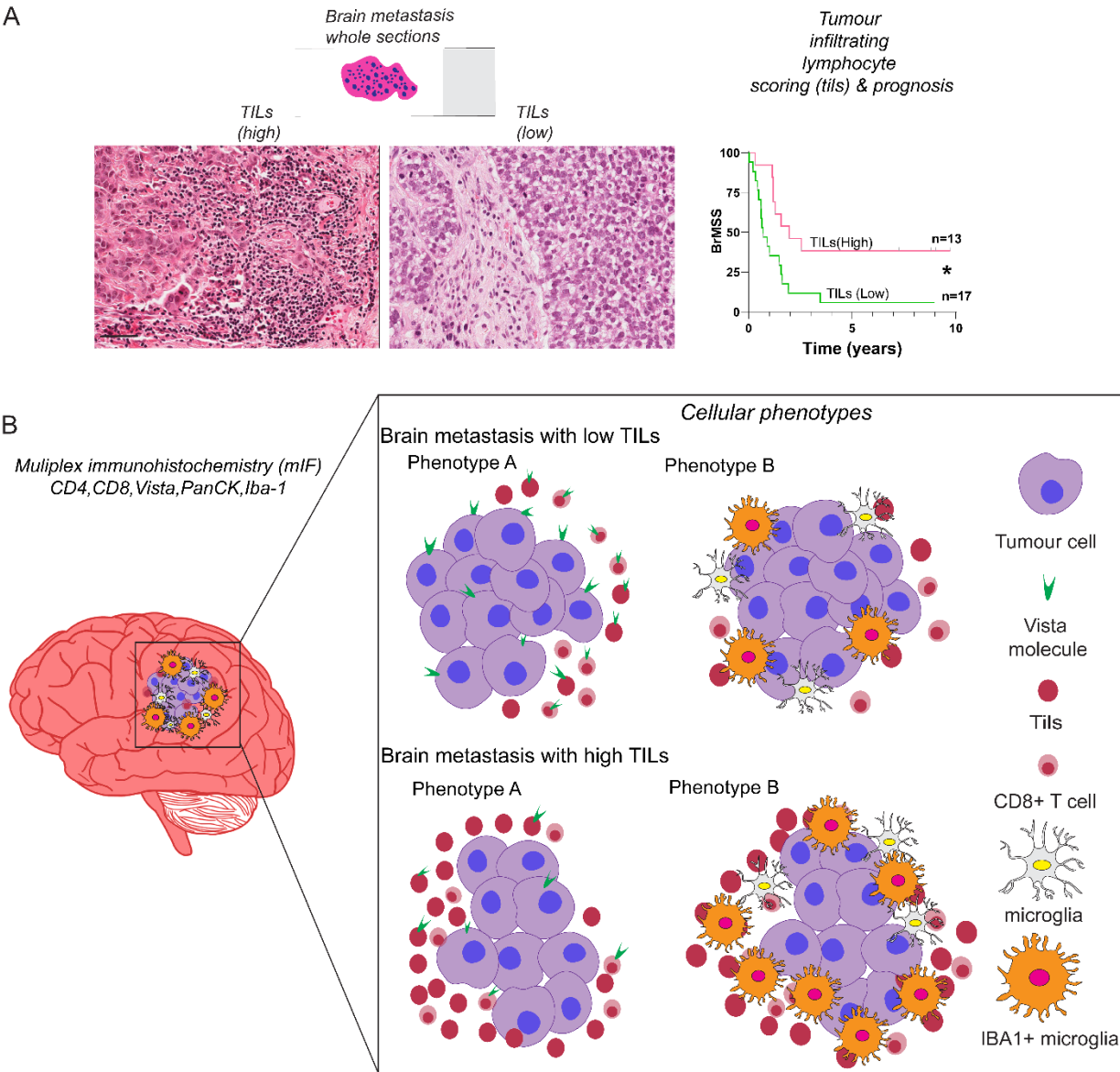
41   **Graphical abstract: Brain metastasis patients with low TILs have high VISTA expression and**
42   **patients with high TILs have significantly more activated microglia**

1. Introduction

Metastatic tumours to the brain, which originate from extracranial primaries such as melanoma, breast and lung remain a significant clinical challenge. Life expectancy of patients after being diagnosed with brain metastases (BrM) can be measured in months [1] and BrMs make up a significantly higher proportion of adult brain tumors compared to primary brain tumours. Currently the gold standard for treating BrMs is surgery, chemotherapy, and radiotherapy. The advent of immunotherapies and their proven efficacy in a subset of BrM patients [2-4] has provided new hope for further therapeutic intervention. However, treatment alternatives still remain limited due to the lack of our comprehensive understanding of the heterogeneity of the microenvironment of the brain. This brain tumor microenvironment (TME) comprises various cell types that can regulate progression of the cancer and also response to therapy [5]. Given the unique adaptations of the brain TME [6-11] as well as the presence of uncommon cell types; microglia (MG), neurons, and astrocytes; and, the blood-brain barrier, makes it compelling to further address the critical question of how TME heterogeneity affects therapeutic efficacy.

Recent work has compared the immune landscape of BrMs and gliomas, where distinctive tumor specific features were discovered [12,13]. These ground breaking studies observed more prominent infiltration of lymphocytes and leukocytes in BrMs compared to gliomas. However, targeted interrogation of the subtypes may be helpful in delineating prognostic cell subsets and specific phenotypes of these infiltrating lymphocytes. In light of this biological question, we explored the infiltrating lymphocyte phenotypes of BrMs arising from breast cancers. We undertook a targeted approach of investigating five markers of interest; Pan cytokeratin (PanCK), CD4, CD8, V-domain immunoglobulin suppressor of T-cell activation (VISTA), Iba-1 to elucidate the immune cell subtypes of BrMs that stratify according to the density of the tumor infiltrating lymphocytes (TILs). We utilized multiplex Immuno-Fluorescence (mIF) to address a number of questions in whole BrM sections. Do tumours with low density of TILs display a different phenotype compared to tumor with high density of TILs? Do the T-cell subtypes display any exhausted phenotypes? Does the density of the microglia differ in these tumours? We focused on the expression of the T-cell inhibitor molecule VISTA for our study as it is largely unexplored in BrMs from breast cancers.

VISTA was first identified by Wang and colleagues [14], where they discovered VISTA to have homology to the extracellular domain of B7 ligand programmed death ligand 1 (PD-L1). They found VISTA's expression to be highly regulated on the myeloid antigen presenting cells and this inhibited T-cell proliferation and cytokine production. Since this discovery, knowledge on the role and function of VISTA in many cancers have been uncovered[15-19]. Furthermore, recent reports on mouse models of brain metastasis suggest VISTA blockade along with anti-PD L1 reduces BrM outgrowth and additionally, the release of cytokine Cxcl10 from tumor cells results in recruitment of VISTA expressing myeloid cells leading to T-cell suppression [20].

We interrogated the tumor-intrinsic as well as immune microenvironment specific expression of our marker panel. By exploring a targeted panel of markers within this selected cohort, we discovered that patients with reduced TILs density have increased VISTA+ immune cells as well as tumour cells. This finding enhances our understanding of the immune-suppressive phenotypes of BrM patients with high and low density of TILs. Our study provides a clinical perspective in understanding the association of VISTA expression on the tumor as well as the microenvironment compartment of BrMs using whole tissue sections. This, in turn, may help us uncover new promising, immunotherapies, as well as answer fundamental biological questions related to BrM's immunosuppressive TME.

4. Materials and Methods

Ethics

Ethical approval from the Human Research Ethics Committees of the Royal Brisbane and Women's Hospital (RBWH; 2005000785) and The University of Queensland (HREC/2005/022) were obtained prior to the commencement of this study and de-identified samples were used for all the analyses performed.

We compiled a cohort of brain metastases arising from breast cancers undergoing resection at the Royal Brisbane and Women's hospital, Brisbane, Australia (n=36). Based on the amount of necrosis and tissue availability, we performed multiplex immunofluorescence (mIF) on 20 whole tissue sections from 20 patients.

TILs scoring

Immune cell infiltration was scored within the boundary of the tumor by a Pathologist (WGK). As there is no set diagnostic criteria for scoring TILs in brain metastases, for our research purposes we adapted the Guidelines for TILs assessment from the "International Immuno-Oncology Biomarker Working Group" [21]. Immune infiltrate was quantitated by the area occupied by mononuclear inflammatory cells (lymphocytes and plasma cells) over total stromal area. TILs within the borders, invasive edges and desmoplastic stroma of the metastatic tumors were included in the evaluation. The proportion of TILs within the stromal area was measured in percentage and initially criteria was set as per the guidelines. However, we restratified this criteria to > or < 30% TILs as this showed the best stratification within our cohort.

Transient knockdown

MDA-MB-468 cells were purchased from the American Type Culture Collection (Manassas, VA, USA) and grown under standard culture conditions. Transient knockdowns were performed with mycoplasma free cells using 100 nM siRNAs comprising of three different probes (Gene Pharma, Shanghai, China) and FugeneHD (Promega, Madison, WI, USA) for 24 hours. The cells were fixed in 10% neutral buffered formalin (Sigma-Aldrich, Missouri, USA) after 24 hours and embedded in paraffin for antibody validation by immunohistochemical analysis.

sense（5'-3'）	antisense（5'-3'）
CCGUAUUCCCUGUAUGUCUTT	AGACAUACAGGGAAUACGGT
GCAAAGAUGCACCAUCCAATT	UUGGAUGGUGCAUCUUUGCTT
GCAACAUUCAAGGGAUUGATT	UCAAUCCCUUGAAUGUUGCTT

mIF and IHC

Four-micron thick sections were used to perform mIF for detecting CD4, CD8, Vista, PanCK and Iba-1 using Tyramide Signal Amplification (TSA) (Opal Kit, Perkin Elmer, Waltham, MA, USA) according to the manufacturer's instructions to detect. The sections were processed and the images were acquired using the Vectra 3.0 Automated Quantitative Pathology Imaging System and analysed using InForm software (v2.4.1, Perkin Elmer, Waltham, MA, USA). An average of 11 ROIs per tissue section were utilized to perform the analysis. As the analysis of the study is based on using algorithms to differentiate between the markers, we performed a thorough initial optimization to avoid false double positives. This was at first achieved by optimizing the dilution of the antibodies at different concentrations and on different channels. We found that Vista (1:500, Opal 520), CD4 (1:1000, Opal 570), PanCK (1:200, Opal 620), Iba-1 (1:50000, Opal 650), CD8 (1:1500, Opal 690) gave us the best distinction with no bleed over of the channels. We also trained the InForm software, to avoid nuclei which could be colocalizing and hence

139 ensuring to circumvent any false double positives. Furthermore by using sections of only 4 um in
140 thickness aided us in bypassing colocalized nuclei as usually one nucleus is about 5-6 um.

141

142 IHC was also performed on four-micron whole sections using the MACH1 Universal HRP-Polymer
143 Detection Kit (BioCare Medical, Pacheco, CA, USA) according to the manufacturer's instructions. Briefly,
144 the sections were dewaxed, de-paraffinized and rehydrated in decreasing concentrations of alcohol (100-
145 70%). Heat-induced antigen retrieval was performed using sodium citrate buffer (0.01M, pH 6.0) at 110°C
146 for 10 mins in a decloacking chamber (BioCare Medical). The sections were treated with 0.3% Hydrogen
147 peroxide for 30 min to remove endogenous peroxidases and then with MACH1 Sniper blocking reagent
148 (BioCare Medical) to avoid non-specific antibody staining. Primary antibody diluted in DaVinci Green
149 Diluent (BioCare Medical) was applied to the sections and the slides were incubated for 3.5 hrs at RT in
150 a humidified slide chamber. MACH-1 anti-rabbit secondary antibody conjugated to horseradish
151 peroxidase was applied for 30 min at RT followed by the Diaminobenzidine (DAB) chromogen substrate
152 for 5 min. The slides were counterstained with Hematoxylin for 4 min and cover-slipped using the DPX
153 mountant (Sigma Aldrich, St Louis, MO, USA). For analysis, the slides were scanned using the Aperio
154 AT Turbo (Leica Biosysems, Wetzlar, Germany) at 40x magnification.

155 **Dataset analysis**

156 Raw gene counts were initially filtered, removing any gene with less than 1 count per million in at
157 least 2 samples. The raw data was subsequently normalized using the trimmed mean of M values (TMM)
158 approach using the edgeR package, resulting in an expression matrix with 226 samples and 18735 genes.
159 To rank the expression of VISTA, genes within each sample were sorted according to their expression;
160 with the genes having the highest expression receiving the highest rank and vice versa for the gene with
161 the lowest expression. To account for ties in rank between genes, if two or more genes had the same rank,
162 then, their rank was replaced by the average of their initial rank. To perform the ranking, the rank function
163 in base R was used , with default parameters.

164 **Statistical analysis**

165 All statistical analysis and the preparation of graphs were achieved by using GraphPad Prism
166 software(v8.2). The data were analyzed using non-parametric t-tests with p-values <0.05 considered to be
167 significant.

168 **2. Results**

169 **Cohort description and image cytometry**

170 In this selected cohort, the median age at which the primary breast cancer was diagnosed was 45
171 years, with brain metastasis diagnosis at 47 years; median time to develop brain metastasis was 25 months
172 from primary diagnosis. Half of the analysed patients within this study (53%) had triple-negative BC -
173 (TN)) followed by HER2+; 34% and ER+; 13% (Figure-1a). These breast cancers were also high grade with
174 56% patients falling into grade 3 category and 24% in grade 2 (Figure-1b). The tumor infiltrating
175 lymphocytes were scored according to the International TILs working group [21], and we restratified the
176 groups into TILs density criteria based upon (>30%, high or <30%, low) (Figure-1c) This segregation was
177 significantly prognostic (p<0.01) for brain metastasis specific survival (BrMSS) with a hazard ratio of 2.9
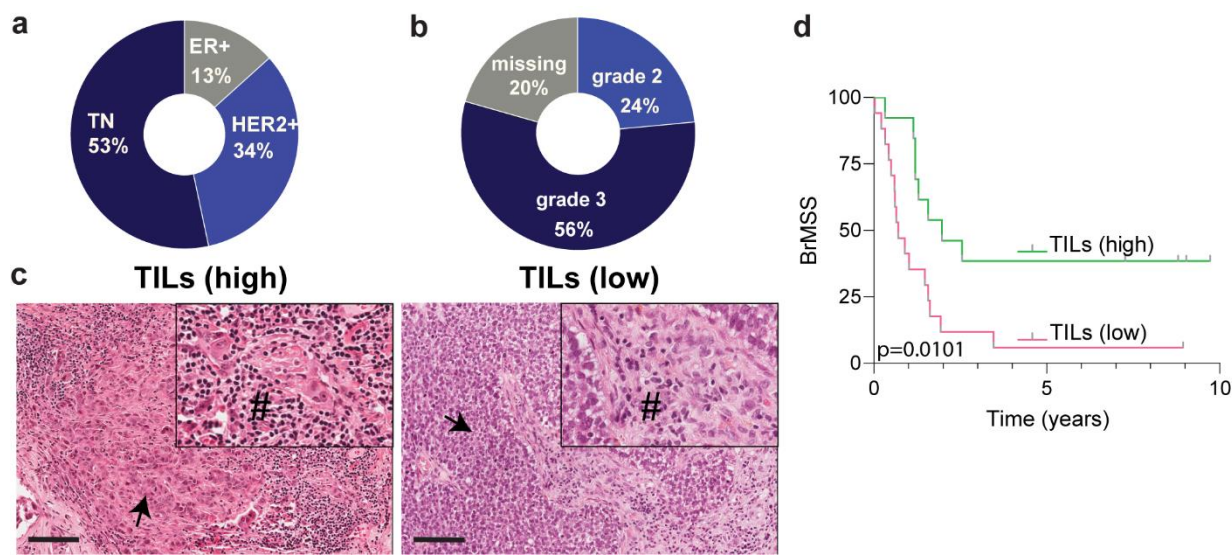178 (Figure-1d).

179
180

Figure 1. Cohort demographics and survival analyses. (**a**) Subtype breakdown of the primary breast cancers giving rise to the brain metastases; (**b**) Tumor grade breakdown of the cohort; (**c**) Hematoxylin and eosin stained representative image for TILs scoring and grouping; (**d**) Kaplan-Meier curve analysis showing brain metastasis specific survival of the TILs high and TILs low groups; *# TILs; arrows indicate tumor. Scale bar 100 μm.*

186

187

188   We performed transient knockdown of *VSIR* gene on the breast cancer cell line MDA-MB-468 to test
189   the specificity of VISTA antibody. Antibodies against the other markers were extensively used and well
190   characterised hence, eliminating the need to re-validate them. As demonstrated in Figure 2a, at high and
191   low magnification we observe positive staining for VISTA protein in the cells that received scrambled
192   control sequence. Contrastingly, in the cells that received the short interfering RNA sequence against
193   *VSIR* we observe no staining at the protein level. After validation of the antibody, we performed multiplex
194   immunofluorescence (mIF) labelling using tyramide signal amplification (TSA) to profile CD4, CD8,
195   VISTA, Pan cytokeratin (PanCK) and Iba-1 positive cell subsets within this cohort. Images were acquired
196   on the Vectra automated quantitative digital pathology platform and data was processed using InForm
197   software's standardized workflow tool . Spectral unmixing precisely separated the staining patterns of
198   each different protein by employing the distinctive features of the dyes and was performed to ensure no
199   bleed through or overlapping of the adjacent fluorochromes (Figure-2b) thus limiting false positive
200   results. Representative images of the separation of DAPI, PanCK at 620 nm, CD4 at 570 nm, Iba-1 at 650
201   nm, CD8 at 690 nm, and VISTA at 520 nm are shown in Figure-2b; a clear distinction of the cellular subsets
202   is observed at the different wavelength channels for each marker. Following tissue and cell segmentation,
203   we integrated the respective segmentation dataset employing the FCS express 6 cytometry software. This
204   enabled us to analyze the multiplexed images from 10-15 randomly selected regions of interest for each
205   case (Figure-2c). We quantified the multi-parameter spatial (different regions of the tumor)- as well as
206   single-cell cluster phenotypes within our dataset. The data was at first scrutinized at the tissue level with
207   tumor and tumor-associated area/stroma separated on a histogram (Figure-2c). We also visualized the
208   data on histograms for each tissue region to separate the CK+ (tumor/epithelial cells) and CK- (non-tumor
209   cells), followed by CD8+ and CD4+ subsets (Figure-2c). Approximately 15 000 cells per case were analyzed
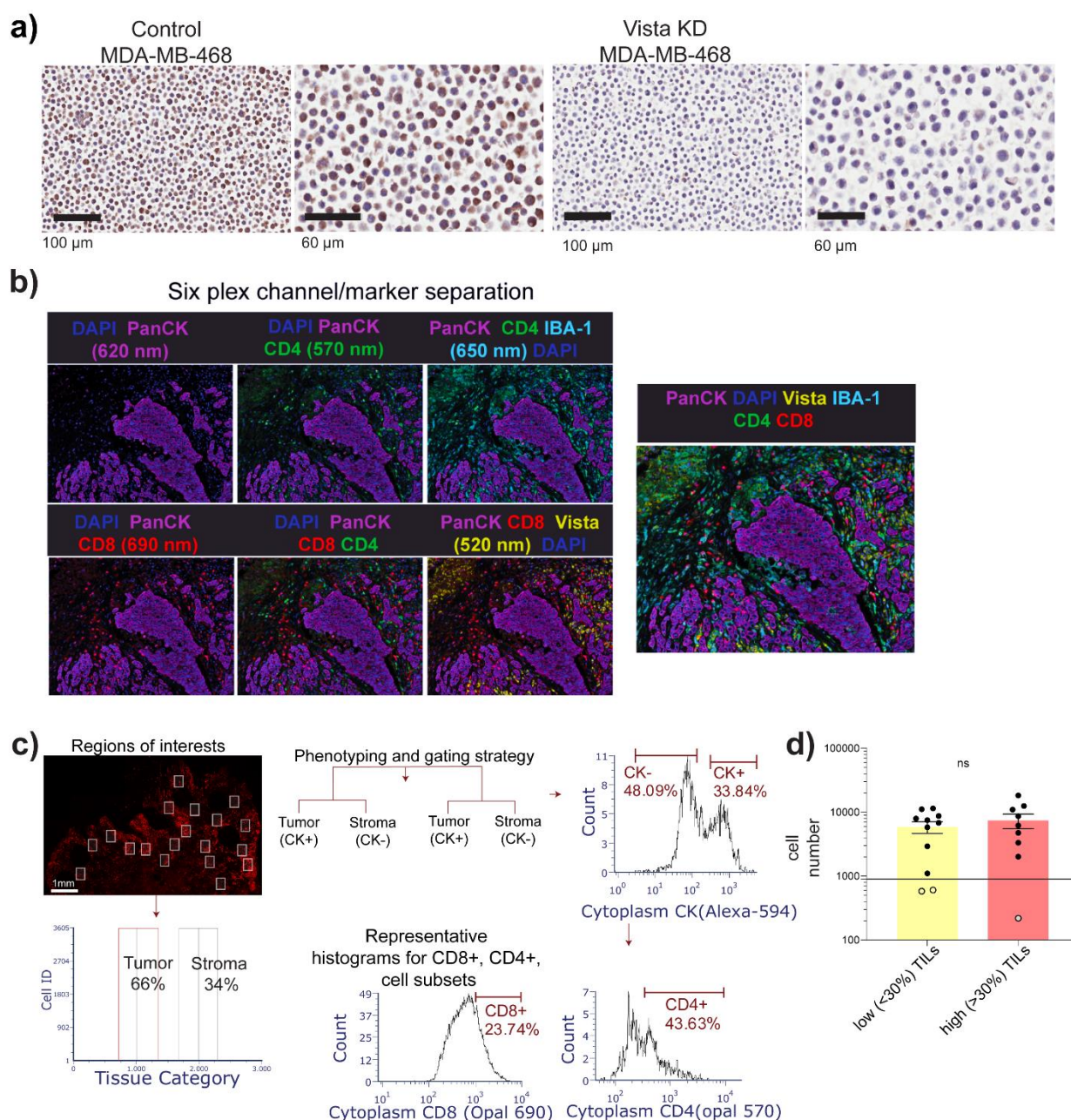210   per case (Figure-2d).

Figure 2. Imaging, tissue, and cell segmentation. **a**) VISTA antibody validation on MDA MB 468 cells using IHC using scrambled control and siRNA against *VSIR* gene b) Spectral unmixing and separation of the fluorochromes highlighting the different cell subsets; (**c**) Data integration and representative gating strategy for single-cell subset analysis in different regions of the samples; example of the ROIs in a case followed by separation of the tumor and stroma regions based on PanCK expression. These parent cell populations were further gated for CD8 ,CD4+ cell subsets (d) Average cell numbers from each group being analysed in the study; each dot is representing a case.

Increased VISTA and Iba-1 expression in the TME

We segmented the tissue regions into tumor and stroma and analysed each compartment to delineate cellular phenotypes. We considered cells showing positive expression of PanCK to be tumor epithelial cells and quantified the subset of TILs as indicated in Figure 2c. Initially we considered single marker positive cell subsets and found that VISTA was expressed on the tumor cell surface in all samples however, the proportion of VISTA+ tumor cells differed between the groups (Figure-3a).The percentage

225 of tumor cells that expressed VISTA on their surface was 50% in the low TILs group compared to 23% in
226 the high TILs group (p=0.0027; Figure-3a).
227   We also found its exclusive expression in 27% of the low TILs group, which was significantly higher
228 than 19% in the high TILs group (p=0.0320; Figure-3b). Interestingly, VISTA has been reported to be
229 highly expressed by microglia and especially differentially expressed in central nervous system (CNS)
230 pathologies [22]. Therefore, we next asked if there was an association between VISTA and the microglial
231 marker Iba-1 expression in the TME. VISTA and Iba-1 co-expression was found to be present in about
232 25% of the microglia (Suppl Figure-1i). Interestingly, 40% of both groups displayed negativity for all the
233 markers used in the study (Suppl Figure-1ii). As the presence of microglia in the brain TME has been
234 previously described [23] and we also investigated if there was a difference in the proportion of microglial
235 cells between low and high TILs groups. We observed that 60% of the TME cells were Iba1+ in the high
236 TILs group (p=9.9 x 10^{-6}; Figure-3b) compared to 30% in the low TILs group.
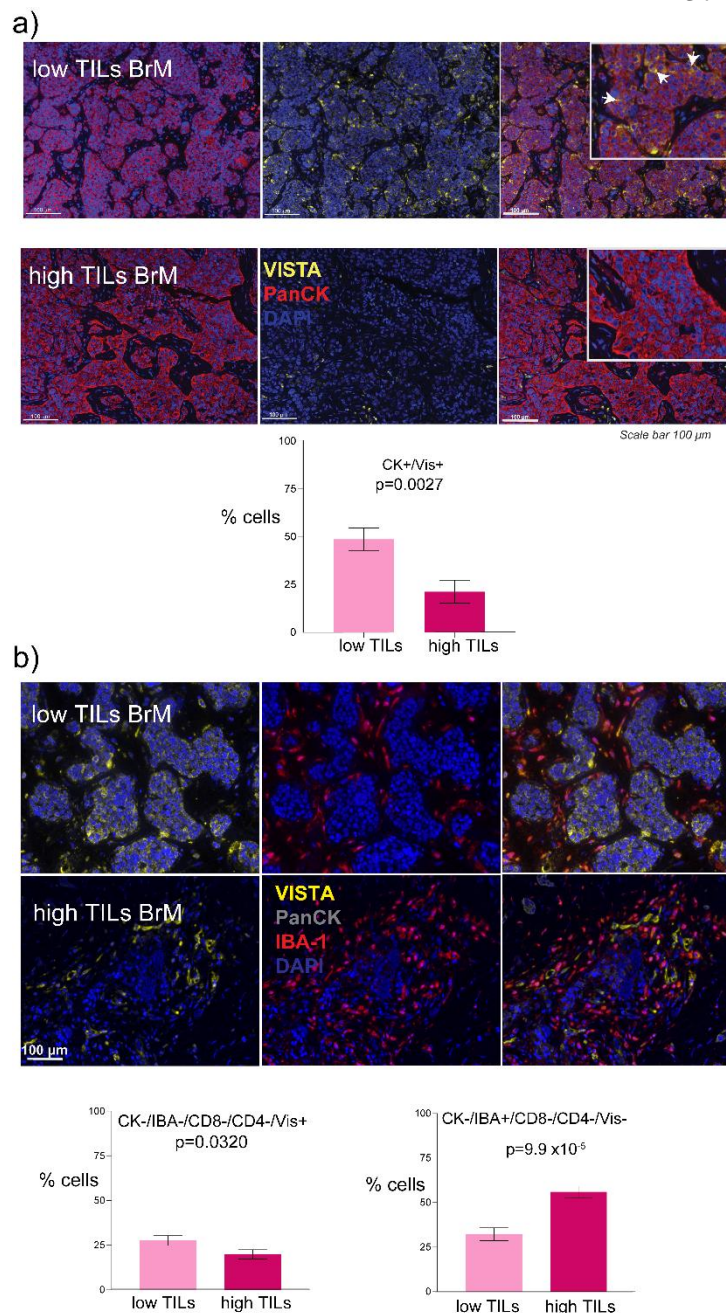237

Figure 3. VISTA and Iba1+ cellular subtypes a) VISTA expression on the tumor cell surface of the low *vs.* high TILs groups and the associated bar graph; arrows indicate vista positive tumor cells (b) Images represent the expression of VISTA and Iba1+ cells and bar graphs showsVISTA and IBa1+ exclusive cells Between the low and high TILs groups respectively.

255

256

Phenotypes of the CD8+ T cells

We investigated the CD8+ and CD4+ T-cell phenotypes in our cohort. The CD4+ T cells did not differ significantly in their proportion in low and high TILs groups, 30% of CK- cells were CD4+ in the low TILs and 38% in the high TILs group (Suppl Figure-1iii). We also found 37% and 40% of CD4+ cells co-expressed Iba-1 (Suppl Figure-1iv). Double positive subsets within CD4+ T cell population such as Iba-1+/VISTA+ or IBA-1+/VISTA- were found to be similar in their proportions in both the groups (Suppl Figure1v, vi, vii, viii). In tumors with high and low TILs (Figure-4a), 25% and 26% of CK- cells were CD8+ T-cells respectively (Figure-4b). Interestingly, this changes for double positive cells; where 46% of CD8+/Iba-1+ are found to be present in the high TILs groups compared to 26% in the low TILs (p=0.0110; Figure-4c). We investigated if this was true when triple positive populations were analysed and this pattern remained the same with high TILs group displaying higher (49%) CD8+/Iba-1+/VISTA- population (p=0.0463; Figure-4Aiv). When we examined VISTA expression within CD8+ population (Figure-4e) we found 30% of CD8+ T cells express VISTA in the low TILs group compared to 18% in the high TILs group (p=0.0080; Figure-4f). Intriguingly, when we investigated Iba-1 positivity within CD8+/VISTA+ population, we found a similar trend with CD8+/Vis+/Iba-1+ or Iba-1- cells; where low TILs group had higher amount of both populations 44% (p=0.0021; Figure-4g) and 26% (p=0.0092; Figure-4h) compared to high TILs tumors respectively.
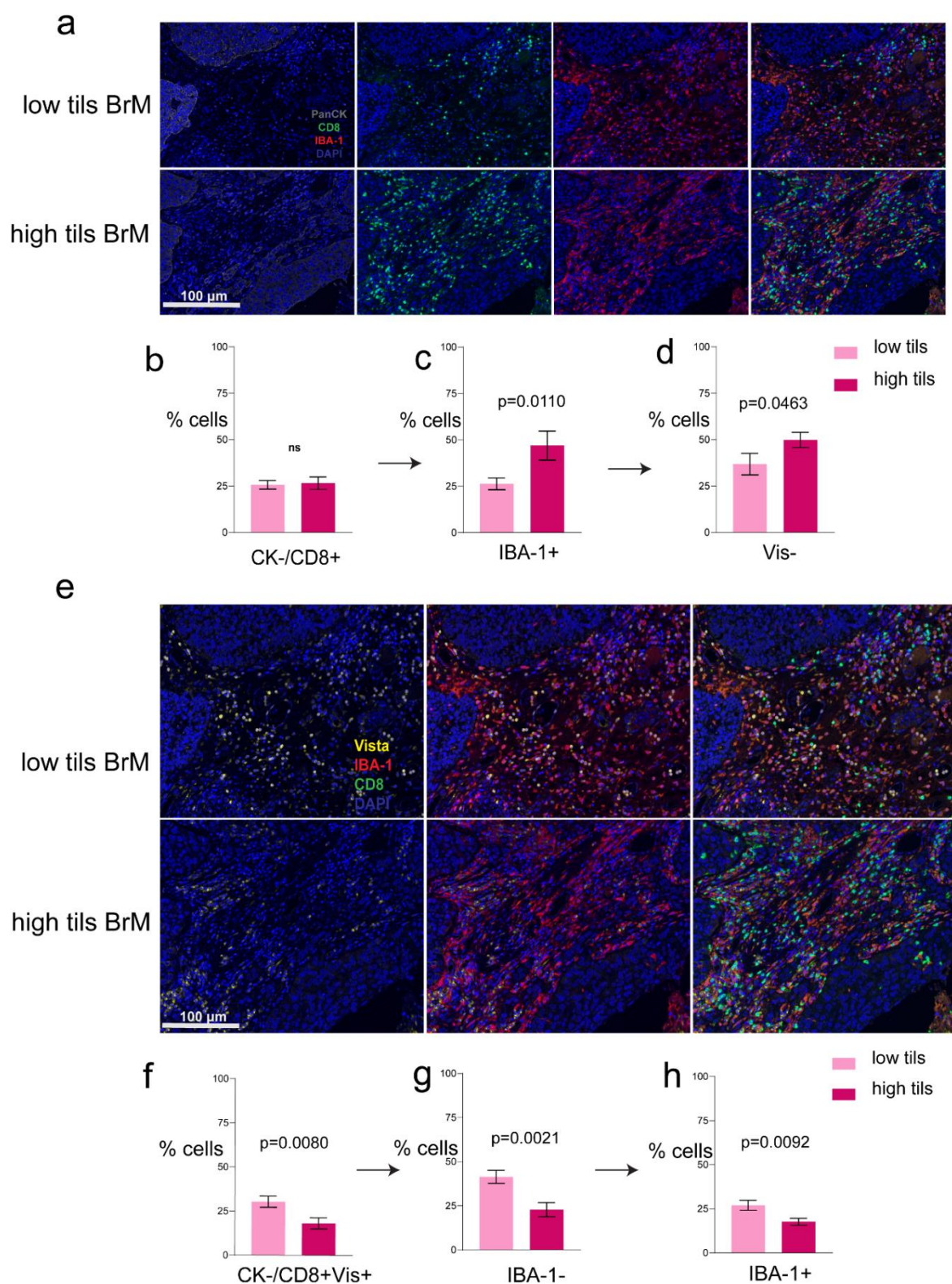
Figure 4. CD8+ T cell populations with arrows indicating the direction of the subsequent gated cell populations within the parent population a) Representative images of mIF :CK, CD8, and Iba-1; b) CD8+ gated population of cells comparison between the low and high TILs groups; c) Bar graphs showing Iba-1+ cells within the CK-/CD8+ parent population; d)VISTA negative cells within the CK-/CD8+/Iba-1+ cells; e) Representative images of mIF : CD8, VISTA and Iba-1; f) CK-/CD8+ gated parent population with VISTA expression; g) Bar graphs showing Iba-1- cells within the CK-/CD8+Vis+ parent population; h)Iba-1+ cells within the same parent population

Validation of mIF using IHC and RNA expression analysis

After quantifying the phenotype of the TILs using mIF, we next attempted to validate our findings using standard immunohistochemistry of VISTA, Iba-1, CD4 and CD8 on eight randomly selected whole sections; four from low TILs and four from high Tils within our cohort. Upon semi-quantitative scoring, Vista was positively stained on the tumor cells for three out of four cases in the low TILs group. In the high TILs tumor no tumor cell positivity was evident on single IHC for VISTA (Figure-5a). Iba-1 (Figure-5a) was also found to be highly expressed in the TME of high TILs BrMs compared to low TILs (Figure-5a). We also observed similar pattern of positive staining for CD8 and CD4 in the TME in low and TILs tumors with no evident difference (Figure-5a). To further delineate the expression of VISTA in BrMs, we explored the Klemm dataset [12], where after flow cytometry assisted separation of immune cell and non-immune cells, they performed RNA-sequencing on BrMs and glioma samples. We examined the expression of *VSIR* in BrMs and gliomas in the non-immune (CD45-) population and found BrM non-immune cells to have a significantly higher level of VISTA expression (p=0.0453; Figure-5b). Ranking of VSIR gene within the CD8+ population in BrMs revealed that in 75% of cases, VISTA's abundance is in the top 10 percentile (top quartile) of all ~18000 genes expressed in this cell subtype (Figure-5c). We also compared the expression of *VSIR* in the microglial (MG), monocyte-derived macrophages (MDMs) and non-immune population (CD45-) within BrMs. Interestingly, we found that in BrMs *VSIR* expression was significantly higher in the cells from myeloid lineage, especially microglia (Figure-5d). This population had significantly higher expression of *VSIR* compared to CD8+ (p=0.043; Figure-5d) as well as CD45- cells (p<0.000001; Figure-5d). The expression levels were comparable between the MDMs and CD8+ cells, however, *VSIR* expression was higher in MDMs compared to CD45- cell (p<0.000001; Figure-5d).
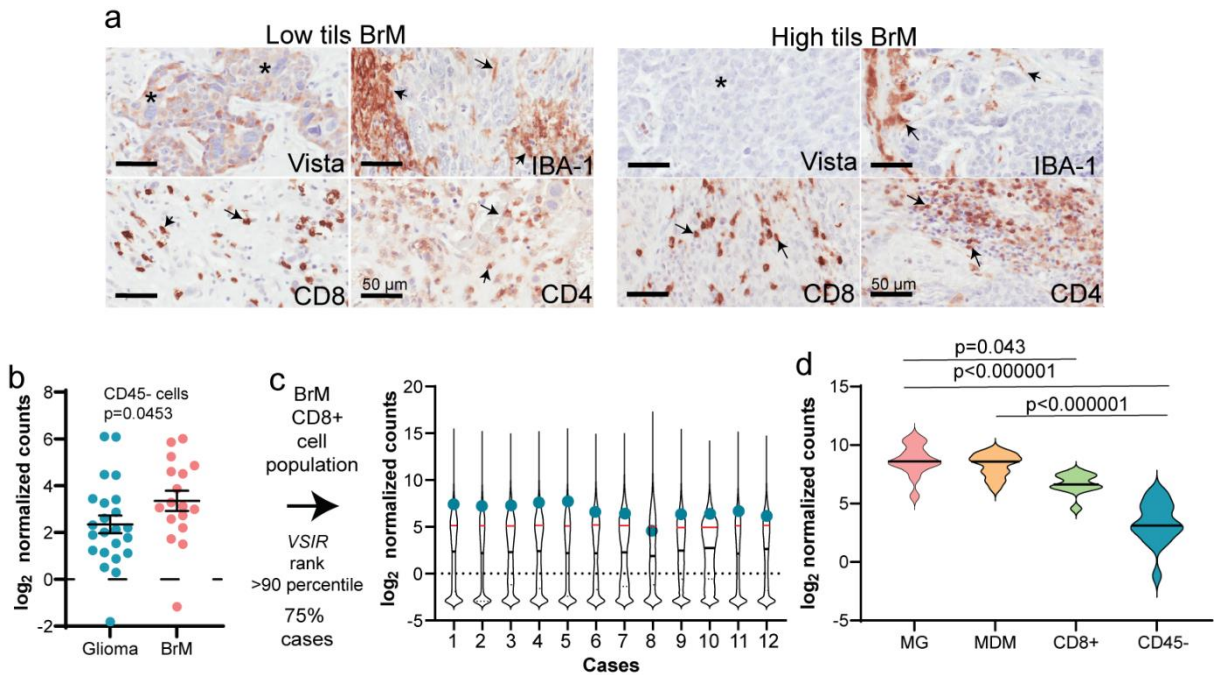

Figure 5. VISTA expression analysis using single IHC as well as RNA analysis in the Klemm dataset. (a) Representative images of standard IHC staining on BrMs sections with * representing tumor cells and arrows indicating positive staining. (b) *VSIR* gene expression in BrMs and Gliomas within CD45- population in the Klemm RNAseq dataset [12]; (c) Ranking of VSIR in CD8+ population within BrM cases;(d) Within BrMs expression levels of VSIR in Microglial (MG), monocyte-derived macrophages (MDMs), CD8+ and CD45- populations.

3. Discussion

The brain TME is a rapidly evolving field of research and its importance is widely recognized as a critical regulator of progression and treatment resistance. In spite of emerging data associating tumor infiltrating lymphocytes to prognosis in BrMs [24-26], the immune cell subsets and phenotypes within BrM are not well-defined. We analyzed by employing a mIF approach, a targeted panel of immune-related proteins; CD4, CD8, Iba-1, and VISTA which have not yet been described in brain metastasis in either the single- or co-expression context. We specifically investigated the CD8+ and CD4+ T cells and compared their phenotypes in BrMs with high and low infiltrating lymphocytes which were also prognostic. We interrogated how the TILs in patients with better prognosis differ in their phenotype compared to the ones with poor prognosis within our selected cohort.

Our data showed that VISTA is highly expressed on the tumor cell surface of BrMs and this was significantly higher in the group with low density of TILs. Overall, we observed an enhanced expression of VISTA in the tumor compartment as well as in the microenvironment of patients with low density of TILs. Interestingly these patients also had a poorer prognosis compared to the high TILs group. In this setting, VISTA might be manifesting immune-modulatory effects, especially in tumours with low density of TILs. However, we cannot eliminate the possibility that VISTA expression on the tumor cell surface may have caused less TILs to infiltrate the area.

VISTA is a negative immune checkpoint regulator, is highly expressed in myeloid cells and its expression is known to be suppressive on resting as well as activated CD4+ and CD8+ T-cells [27]. Our findings on VISTA being expressed by epithelial cells confirms data in other cancers [19,27-31]. In non-small cell lung carcinomas (NSCLC), VISTA was found to be expressed in majority of NSCLCs and contrastingly this expression associated with lymphocyte infiltration and PD-L1 expression [28]. In ovarian cancer, expression of VISTA has contradicting reports. On one hand two studies indicate VISTA to be highly enriched in tumors leading to a poor prognosis and advanced disease and on the other, one study has been shown VISTA to be associated with good prognosis. Mulati and colleagues found VISTA to be expressed in 91% of the samples and in an animal model bearing ovarian tumours, anti-VISTA antibody increased the longevity of the treated animals by reducing the tumor burden. In-vitro studies showed that tumor cell expression of VISTA caused immune evasion by suppressing T-cell proliferation and cytokine production [27]. Additionally, VISTA expression has been linked to the progression of the disease in ovarian cancers. The authors noted that expression of VISTA increased with advanced disease and lymph node metastasis [19]. Contrastingly, VISTA's expression has also been shown to associate with a favorable prognosis in a different cohort of high-grade ovarian cancers. This retrospective study had used tissue microarrays to assess the expression of VISTA on tumor cells as well as in immune cells [31]. These two studies had different scoring criteria, and the study by Liao and colleagues used whole sections which might have provided a higher accountability for the heterogeneity within the section. Nevertheless, more in-depth analysis is required to understand the contrasting associations of VISTA in ovarian cancer. Our observation of co-expression of VISTA on CD8+ T cells on low TILs density can also be extrapolated to suggest that perhaps VISTA expression is causing immune evasion.

With respect to Central Nervous System metastatic disease, recent work by Guldner and coworkers have identified brain resident myeloid cells to be inducing an immunosuppressive microenvironment, thus promoting metastasis [20]. This study generated mouse models of BrMs to derive functional understanding of the myeloid cell population in this disease. When they performed mechanistic in-vitro and in-vivo studies they found C-X-C motif chemokine ligand 10 (Cxcl10) promoted BrMs, and as this chemokine is an immune modulator, they further characterized to elucidate the mechanism behind it. Investigation of publicly available human CNS myeloid RNAseq datasets, they found increased expression of Vsir (VISTA) and CD274 (PD-L1) in the myeloid cells [20]. In addition, they found co-inhibition of PD-L1 and VISTA in a mouse model of brain metastasis reduced the metastatic burden. Our results are complimentary to their finding where we have shown increased VISTA in a sub-population of patients with BrMs and its expression is an indicator of poor prognosis. Furthermore, we observe an enhanced expression of VISTA in BrMs compared to gliomas as well as VISTA was more pronounced in the myeloid lineage cells in our mIF study as well as in the Klemm dataset [12]. To our knowledge our

363 study is the first to show this differential expression of VISTA in the tumor as well as in CD8+ T cells in a
364 BrM clinical cohort.

365 Brain resident macrophages/microglia perform numerous roles in brain health and disease [32]. With
366 respect to BrMs, microglia are known to be multifaceted in their function such as promoting proliferation,
367 angiogenesis and invasion in BrMs [33]. Recent work by Simon and co-workers, highlighted using intra-
368 vital microscopy how microglia are recruited and activated after xenotransplantation of breast cancer
369 cells into the brain [34]. This study showed that microglial activation and accumulation around the lesion
370 can cause infiltration of immune cells as well as aberrant electrical activity in the brain. Similarly, in a
371 mouse model of BrM, microglial accumulation has been associated with increased tumor burden. When
372 selective depletion of the anti-inflammatory microglial phenotype was carried out, a reduction in tumor
373 burden was observed [35]. These studies highlight the importance or microglia in brain metastasis. For
374 this study we used a common microglial marker Iba-1 in our panel to investigate the expression levels
375 and associations of Iba-1+ microglia.

376 Our findings suggest increased microglia in the tumours with high density of TILs and we also
377 observe increased CD8+ T-cells that co-express Iba-1. Simultaneous accumulation of microglia and
378 infiltration of immune cells has been shown in a mouse model of BrM [34]. Although no mechanism is
379 known for this association, this accumulation was found to reduce the density of tumor cells in the brain
380 [34]. We observed increased microglia in the high TILs group which also had a better prognosis. This
381 suggests that perhaps increased microglia may have caused anti-tumour immunity. Additionally, our
382 perplexing finding of double positive CD8+/Iba-1+ cells, leads us to suggest that these double positive
383 cells may be representing pro-inflammatory M1 macrophages. This is plausible because Boddaert and
384 colleagues used a rat model for stroke to demonstrate increased CD8 expression in activated macrophages
385 using Iba-1 as a marker. Their results corroborate our finding of double-positive macrophages.
386 Furthermore, in-vitro analysis revealed CD8 stimulation caused repolarization of M2 to M1 phenotype
387 along with highly proliferative Iba-1+CD8+ cells [36]. If this is true for our findings, then this co-
388 expression could play a protective role in BrMs. It is known that microglia can exist in two states, anti-
389 inflammatory which facilitates invasion, angiogenesis and tumour growth [33,37]; and pro-inflammatory
390 which can release proinflammatory cytokines, eliciting a T-cell response [38]. Pro-inflammatory
391 microglial phenotype switch can infer a microglial population which may have caused anti-tumor
392 immune response[39]. Nonetheless, we cannot rule out the possibility of false double positive cells,
393 however we strongly believe this is highly unlikely. Future studies are required to investigate a larger
394 population of resected tumors using flow cytometry to see if double positive CD8+/Iba-1+ are a consistent
395 phenotype in BrM.

396 We appreciate the limitations of this study such as the size of the cohort which needs to be expanded
397 to further validate our findings. We have used commercially validated antibodies however, batch
398 variability might still play a role and therefore, future studies should focus on employing various
399 commercially available antibodies to test the suggested phenotypes of TILs in BrM from this body of
400 work. In addition, we cannot eliminate the effect of treatment that may be impacting the TILs phenotype
401 as our patient population ranges from early to late 2000s and the treatment regimen has drastically
402 changed within the last decade. For example, it would be crucial to test Vista expression in a patient
403 population treated with current immunotherapy regimens as that might provide novel insights into
404 treatment response. Furthermore, BrMs arising from different primaries may have different phenotypes
405 which need to be further elucidated. Finally the functional implications of these findings using different
406 in-vitro and in-vivo models would be essential in the future for clinical translation.

407 Overall, we have utilized mIF as a tool to provide a proof of concept study to demonstrate TME
408 distinctive changes in the TILs of BrM. Through this we have defined the expression of a new immune
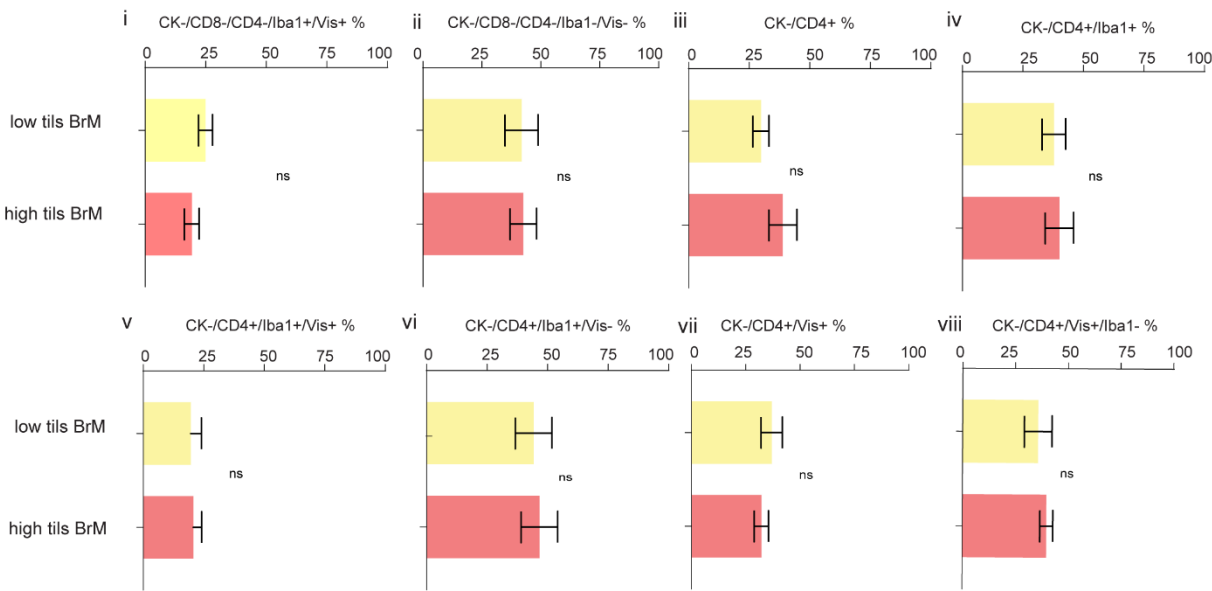409 checkpoint molecule in a clinical cohort of BrMs.

410 5. Conclusions

411 Brain metastasis from the breast is one of the common causes of mortality in women, the poor quality
412 of life and the associated morbidity makes it compelling to understand the disease better. An emerging
413 and evolving concept within the brain TME is the existence of the complex landscape of cells within this

414   unique organ. The positive brain tumor responses to immune checkpoint inhibition raises optimism that
415   extensive understanding of the biology of the tumor will lead to better management. There is hope that
416   developing a comprehensive understanding of the TME will lead to design of more effective
417   immunotherapies. Our study has, shown a novel immune checkpoint, VISTA, to be highly expressed in
418   brain metastasis and its expression is higher in the group of patients who have a worse prognosis
419   compared to the high TILs group. We have also provided insights into the VISTA co-expressing immune
420   cell subsets within our selected cohort. We found increased microglia to be more pronounced in BrMs
421   with high density of TILs and we also observed CD8 + Iba-1 cells. Further studies are required to elucidate
422   the mechanisms of differential expression of VISTA and microglia in BrMs.

423   **Supplementary Materials:**, Figure S1: Quantified bar graphs of CD4+ subsets within the groups.

424   **Figure S1.** Quantified bar graphs of CD4+ subsets within the groups.
425

426

427
428

429

References

1. Cagney, D.N.; Martin, A.M.; Catalano, P.J.; Redig, A.J.; Lin, N.U.; Lee, E.Q.; Wen, P.Y.; Dunn, I.F.; Bi, W.L.; Weiss, S.E., et al. Incidence and prognosis of patients with brain metastases at diagnosis of systemic malignancy: a population-based study. *Neuro Oncol* **2017**, *19*, 1511-1521, doi:10.1093/neuonc/nox077.

2. Tawbi, H.A.; Forsyth, P.A.; Algazi, A.; Hamid, O.; Hodi, F.S.; Moschos, S.J.; Khushalani, N.I.; Lewis, K.; Lao, C.D.; Postow, M.A. Combined nivolumab and ipilimumab in melanoma metastatic to the brain. *New England Journal of Medicine* **2018**, *379*, 722-730.

3. Long, G.V.; Atkinson, V.; Lo, S.; Sandhu, S.; Guminski, A.D.; Brown, M.P.; Wilmott, J.S.; Edwards, J.; Gonzalez, M.; Scolyer, R.A. Combination nivolumab and ipilimumab or nivolumab alone in melanoma brain metastases: a multicentre randomised phase 2 study. *The Lancet Oncology* **2018**, *19*, 672-681.

4. Hendriks, L.E.L.; Henon, C.; Auclin, E.; Mezquita, L.; Ferrara, R.; Audigier-Valette, C.; Mazieres, J.; Lefebvre, C.; Rabeau, A.; Le Moulec, S., et al. Outcome of Patients with Non-Small Cell Lung Cancer and Brain Metastases Treated with Checkpoint Inhibitors. *J Thorac Oncol* **2019**, *14*, 1244-1254, doi:10.1016/j.jtho.2019.02.009.

5. Jin, M.Z.; Jin, W.L. The updated landscape of tumor microenvironment and drug repurposing. *Signal Transduct Target Ther* **2020**, *5*, 166, doi:10.1038/s41392-020-00280-x.

6. Sevenich, L.; Bowman, R.L.; Mason, S.D.; Quail, D.F.; Rapaport, F.; Elie, B.T.; Brogi, E.; Brastianos, P.K.; Hahn, W.C.; Holsinger, L.J., et al. Analysis of tumour- and stroma-supplied proteolytic networks reveals a brain-metastasis-promoting role for cathepsin S. *Nat Cell Biol* **2014**, *16*, 876-888, doi:10.1038/ncb3011.

7. Neman, J.; Choy, C.; Kowolik, C.M.; Anderson, A.; Duenas, V.J.; Waliany, S.; Chen, B.T.; Chen, M.Y.; Jandial, R. Co-evolution of breast-to-brain metastasis and neural progenitor cells. *Clin Exp Metastasis* **2013**, *30*, 753-768, doi:10.1007/s10585-013-9576-7.

8. Sartorius, C.A.; Hanna, C.T.; Gril, B.; Cruz, H.; Serkova, N.J.; Huber, K.M.; Kabos, P.; Schedin, T.B.; Borges, V.F.; Steeg, P.S., et al. Estrogen promotes the brain metastatic colonization of triple negative breast cancer cells via an astrocyte-mediated paracrine mechanism. *Oncogene* **2016**, *35*, 2881-2892, doi:10.1038/onc.2015.353.

9. Zhang, L.; Zhang, S.; Yao, J.; Lowery, F.J.; Zhang, Q.; Huang, W.C.; Li, P.; Li, M.; Wang, X.; Zhang, C., et al. Microenvironment-induced PTEN loss by exosomal microRNA primes brain metastasis outgrowth. *Nature* **2015**, *527*, 100-104, doi:10.1038/nature15376.

10. Kalita-de Croft, P.; Lim, M.; Chittoory, H.; de Luca, X.M.; Kutasovic, J.R.; Day, B.W.; Al-Ejeh, F.; Simpson, P.T.; Reed, A.E.M.; Lakhani, S.R., et al. Clinicopathologic significance of nuclear HER4 and phospho-YAP(S-127) in human breast cancers and matching brain metastases. *Therapeutic Advances in Medical Oncology* **2020**, *12*, doi:10.1177/1758835920946259.

473 11. Kalita-de Croft, P.; Straube, J.; Lim, M.; Al-Ejeh, F.; Lakhani, S.R.; Saunus, J.M. Proteomic Analysis of the
474   Breast Cancer Brain Metastasis Microenvironment. *Int J Mol Sci* **2019**, *20*, doi:10.3390/ijms20102524.
475 12. Klemm, F.; Maas, R.R.; Bowman, R.L.; Kornete, M.; Soukup, K.; Nassiri, S.; Brouland, J.P.; Iacobuzio-
476   Donahue, C.A.; Brennan, C.; Tabar, V., et al. Interrogation of the Microenvironmental Landscape in Brain
477   Tumors Reveals Disease-Specific Alterations of Immune Cells. *Cell* **2020**, *181*, 1643-1660 e1617,
478   doi:10.1016/j.cell.2020.05.007.
479 13. Friebel, E.; Kapolou, K.; Unger, S.; Nunez, N.G.; Utz, S.; Rushing, E.J.; Regli, L.; Weller, M.; Greter, M.;
480   Tugues, S., et al. Single-Cell Mapping of Human Brain Cancer Reveals Tumor-Specific Instruction of Tissue-
481   Invading Leukocytes. *Cell* **2020**, *181*, 1626-1642 e1620, doi:10.1016/j.cell.2020.04.055.
482 14. Wang, L.; Rubinstein, R.; Lines, J.L.; Wasiuk, A.; Ahonen, C.; Guo, Y.; Lu, L.F.; Gondek, D.; Wang, Y.; Fava,
483   R.A., et al. VISTA, a novel mouse Ig superfamily ligand that negatively regulates T cell responses. *J Exp Med*
484   **2011**, *208*, 577-592, doi:10.1084/jem.20100619.
485 15. Ge, M.J.; Xu, K.L.; Xu, T.; Tang, Y.N.; Li, Z.Y.; Yan, Z.L.; Sun, H.Y.; Cheng, H.; Zhu, F.; Sang, W., et al.
486   [Expression and Significance of PD-1, TIM-3 and VISTA on T Cell of Acute Myeloid Leukemia Patients].
487   *Zhongguo Shi Yan Xue Ye Xue Za Zhi* **2020**, *28*, 748-752, doi:10.19746/j.cnki.issn.1009-2137.2020.03.006.
488 16. Murga-Zamalloa, C.A.; Brown, N.A.; Wilcox, R.A. Expression of the checkpoint receptors LAG-3, TIM-3 and
489   VISTA in peripheral T cell lymphomas. *J Clin Pathol* **2020**, *73*, 197-203, doi:10.1136/jclinpath-2019-206117.
490 17. Zong, L.; Mo, S.; Yu, S.; Zhou, Y.; Zhang, M.; Chen, J.; Xiang, Y. Expression of the immune checkpoint VISTA
491   in breast cancer. *Cancer Immunol Immunother* **2020**, *69*, 1437-1446, doi:10.1007/s00262-020-02554-3.
492 18. Kato, S.; Okamura, R.; Kumaki, Y.; Ikeda, S.; Nikanjam, M.; Eskander, R.; Goodman, A.; Lee, S.; Glenn, S.T.;
493   Dressman, D., et al. Expression of TIM3/VISTA checkpoints and the CD68 macrophage-associated marker
494   correlates with anti-PD1/PDL1 resistance: implications of immunogram heterogeneity. *Oncoimmunology*
495   **2020**, *9*, 1708065, doi:10.1080/2162402X.2019.1708065.
496 19. Liao, H.; Zhu, H.; Liu, S.; Wang, H. Expression of V-domain immunoglobulin suppressor of T cell activation
497   is associated with the advanced stage and presence of lymph node metastasis in ovarian cancer. *Oncol Lett*
498   **2018**, *16*, 3465-3472, doi:10.3892/ol.2018.9059.
499 20. Guldner, I.H.; Wang, Q.; Yang, L.; Golomb, S.M.; Zhao, Z.; Lopez, J.A.; Brunory, A.; Howe, E.N.; Zhang, Y.;
500   Palakurthi, B., et al. CNS-Native Myeloid Cells Drive Immune Suppression in the Brain Metastatic Niche
501   through Cxcl10. *Cell* **2020**, 10.1016/j.cell.2020.09.064, doi:10.1016/j.cell.2020.09.064.
502 21. Salgado, R.; Denkert, C.; Campbell, C.; Savas, P.; Nuciforo, P.; Aura, C.; de Azambuja, E.; Eidtmann, H.;
503   Ellis, C.E.; Baselga, J., et al. Tumor-Infiltrating Lymphocytes and Associations With Pathological Complete
504   Response and Event-Free Survival in HER2-Positive Early-Stage Breast Cancer Treated With Lapatinib and
505   Trastuzumab: A Secondary Analysis of the NeoALTTO Trial. *JAMA Oncol* **2015**, *1*, 448-454,
506   doi:10.1001/jamaoncol.2015.0830.
507 22. Borggrewe, M.; Grit, C.; Den Dunnen, W.F.A.; Burm, S.M.; Bajramovic, J.J.; Noelle, R.J.; Eggen, B.J.L.; Laman,
508   J.D. VISTA expression by microglia decreases during inflammation and is differentially regulated in CNS
509   diseases. *Glia* **2018**, *66*, 2645-2658, doi:10.1002/glia.23517.
510 23. Soto, M.S.; Serres, S.; Anthony, D.C.; Sibson, N.R. Functional role of endothelial adhesion molecules in the
511   early stages of brain metastasis. *Neuro Oncol* **2014**, *16*, 540-551, doi:10.1093/neuonc/not222.
512 24. Berghoff, A.S.; Fuchs, E.; Ricken, G.; Mlecnik, B.; Bindea, G.; Spanberger, T.; Hackl, M.; Widhalm, G.;
513   Dieckmann, K.; Prayer, D., et al. Density of tumor-infiltrating lymphocytes correlates with extent of brain
514   edema and overall survival time in patients with brain metastases. *Oncoimmunology* **2016**, *5*, e1057388,
515   doi:10.1080/2162402X.2015.1057388.

516   25.   Ogiya, R.; Niikura, N.; Kumaki, N.; Yasojima, H.; Iwasa, T.; Kanbayashi, C.; Oshitanai, R.; Tsuneizumi, M.;
517   Watanabe, K.I.; Matsui, A., et al. Comparison of immune microenvironments between primary tumors and
518   brain metastases in patients with breast cancer. *Oncotarget* **2017**, *8*, 103671-103681,
519   doi:10.18632/oncotarget.22110.
520   26.   Berghoff, A.S.; Ricken, G.; Wilhelm, D.; Rajky, O.; Widhalm, G.; Dieckmann, K.; Birner, P.; Bartsch, R.;
521   Preusser, M. Tumor infiltrating lymphocytes and PD-L1 expression in brain metastases of small cell lung
522   cancer (SCLC). *J Neurooncol* **2016**, *130*, 19-29, doi:10.1007/s11060-016-2216-8.
523   27.   Mulati, K.; Hamanishi, J.; Matsumura, N.; Chamoto, K.; Mise, N.; Abiko, K.; Baba, T.; Yamaguchi, K.;
524   Horikawa, N.; Murakami, R., et al. VISTA expressed in tumour cells regulates T cell function. *Br J Cancer*
525   **2019**, *120*, 115-127, doi:10.1038/s41416-018-0313-5.
526   28.   Villarroel-Espindola, F.; Yu, X.; Datar, I.; Mani, N.; Sanmamed, M.; Velcheti, V.; Syrigos, K.; Toki, M.; Zhao,
527   H.; Chen, L., et al. Spatially Resolved and Quantitative Analysis of VISTA/PD-1H as a Novel
528   Immunotherapy Target in Human Non-Small Cell Lung Cancer. *Clin Cancer Res* **2018**, *24*, 1562-1573,
529   doi:10.1158/1078-0432.CCR-17-2542.
530   29.   Rosenbaum, S.R.; Knecht, M.; Mollaee, M.; Zhong, Z.; Erkes, D.A.; McCue, P.A.; Chervoneva, I.; Berger,
531   A.C.; Lo, J.A.; Fisher, D.E., et al. FOXD3 Regulates VISTA Expression in Melanoma. *Cell Rep* **2020**, *30*, 510-
532   524 e516, doi:10.1016/j.celrep.2019.12.036.
533   30.   Zong, L.; Mo, S.; Yu, S.; Zhou, Y.; Zhang, M.; Chen, J.; Xiang, Y. Correction to: Expression of the immune
534   checkpoint VISTA in breast cancer. *Cancer Immunol Immunother* **2020**, *69*, 1447, doi:10.1007/s00262-020-02602-
535   y.
536   31.   Zong, L.; Zhou, Y.; Zhang, M.; Chen, J.; Xiang, Y. VISTA expression is associated with a favorable prognosis
537   in patients with high-grade serous ovarian cancer. *Cancer Immunol Immunother* **2020**, *69*, 33-42,
538   doi:10.1007/s00262-019-02434-5.
539   32.   Hanisch, U.K.; Kettenmann, H. Microglia: active sensor and versatile effector cells in the normal and
540   pathologic brain. *Nat Neurosci* **2007**, *10*, 1387-1394, doi:10.1038/nn1997.
541   33.   Lorger, M.; Felding-Habermann, B. Capturing changes in the brain microenvironment during initial steps
542   of breast cancer brain metastasis. *Am J Pathol* **2010**, *176*, 2958-2971, doi:10.2353/ajpath.2010.090838.
543   34.   Simon, A.; Yang, M.; Marrison, J.L.; James, A.D.; Hunt, M.J.; O'Toole, P.J.; Kaye, P.M.; Whittington, M.A.;
544   Chawla, S.; Brackenbury, W.J. Metastatic breast cancer cells induce altered microglial morphology and
545   electrical excitability in vivo. *J Neuroinflammation* **2020**, *17*, 87, doi:10.1186/s12974-020-01753-0.
546   35.   Andreou, K.E.; Soto, M.S.; Allen, D.; Economopoulos, V.; de Bernardi, A.; Larkin, J.R.; Sibson, N.R. Anti-
547   inflammatory Microglia/Macrophages As a Potential Therapeutic Target in Brain Metastasis. *Front Oncol*
548   **2017**, *7*, 251, doi:10.3389/fonc.2017.00251.
549   36.   Boddaert, J.; Bielen, K.; s Jongers, B.; Manocha, E.; Yperzeele, L.; Cras, P.; Pirici, D.; Kumar-Singh, S. CD8
550   signaling in microglia/macrophage M1 polarization in a rat model of cerebral ischemia. *PLoS One* **2018**, *13*,
551   e0186937, doi:10.1371/journal.pone.0186937.
552   37.   Coniglio, S.J.; Eugenin, E.; Dobrenis, K.; Stanley, E.R.; West, B.L.; Symons, M.H.; Segall, J.E. Microglial
553   stimulation of glioblastoma invasion involves epidermal growth factor receptor (EGFR) and colony
554   stimulating factor 1 receptor (CSF-1R) signaling. *Mol Med* **2012**, *18*, 519-527, doi:10.2119/molmed.2011.00217.
555   38.   Wu, S.Y.; Watabe, K. The roles of microglia/macrophages in tumor progression of brain cancer and
556   metastatic disease. *Front Biosci (Landmark Ed)* **2017**, *22*, 1805-1829, doi:10.2741/4573.

557   39.   Pukrop, T.; Dehghani, F.; Chuang, H.N.; Lohaus, R.; Bayanga, K.; Heermann, S.; Regen, T.; Van Rossum, D.;

558   Klemm, F.; Schulz, M., et al. Microglia promote colonization of brain tissue by breast cancer cells in a Wnt-

559   dependent way. *Glia* **2010**, *58*, 1477-1489, doi:10.1002/glia.21022.

560